Supporting information for:

In-situ Transmission Electron Microscopy Analysis of Copper – Germanium Nanowire Solid-State Reaction

Khalil.El hajraoui,[†,‡] Eric. Robin,[†,¶] Clemens. Zeiner,[§] Alois. Lugstein,[§] Stéphanie.Kodjikian,[†,‡] Jean-Luc. Rouvière,[†,¶] and Martien. Den Hertog[*,†,‡]

†*Université Grenoble Alpes, F-38000 Grenoble, France*

‡*CNRS, Institut NEEL, F-38000 Grenoble, France*

¶*CEA, INAC, F-38000 Grenoble, France*

§*Institute of Solid State Electronics, TU-Wien - Nanocenter Campus Gußhaus, Gußhausstraße 25-25a, Gebäude-CH, A-1040 Wien, Austria*

E-mail: martien.den-hertog@neel.cnrs.fr

Phone: +33 (0)4 76881045

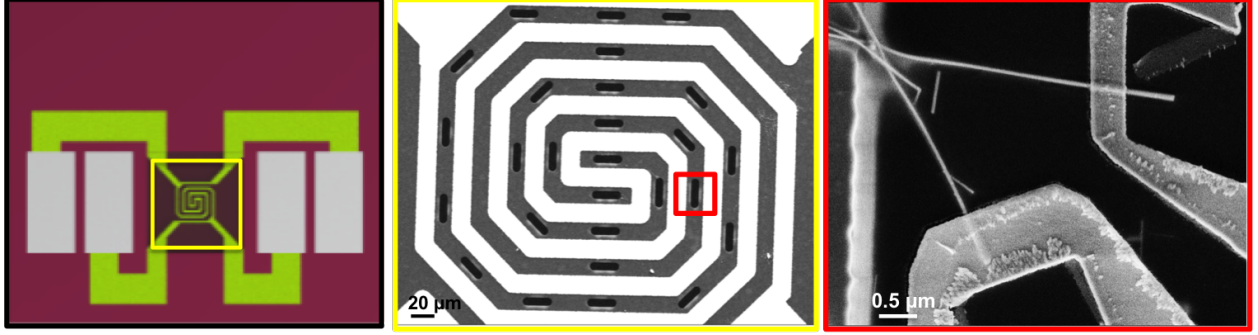Contents

I. Description of heating spiral membranes

Figure S1: a) Photograph of microfabricated commercial membrane from DENS solution calibrated in temperature used during H_b heating experiments. b) SEM image showing a heating spiral and 20 nm thick Si_3N_4 membranes for electron transparency. c) SEM image on a membrane showing an electron lithography contacted Ge NW with Cu metal.
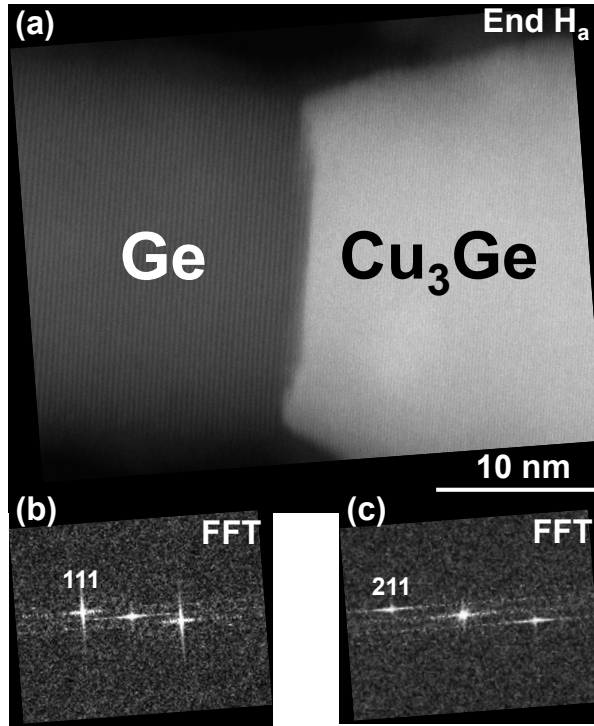
II. Structural and Kinetic analysis

Figure S2: STEM image of a suspended Cu-Ge(NW) solid-state reaction after H_a heating processes. (a) High resolution HAADF STEM image of the Ge/Cu_3Ge interface after a H_a heating process on a holey membrane.(b),(c) The corresponding Fourier Transform patterns of the Ge/Cu_3Ge interface showing the epitaxial relation adapted from.[S1]

Fig.(S2.a) presents High Angle Annular Dark Field (HAADF) STEM image after H_a heating experiments. The contrast in HAADF STEM depends both on the sample thickness and on its composition, where the more heavy elements scatter more electrons on the annular detector, giving rise to a brighter contrast. Therefore, a strong contrast is present on the thicker Cu contacts and on the transformed region due to the change in the NW diameter after copper intrusion compared to the unreacted Ge part. Fig.(S2) represents the high resolution HAADF STEM image and corresponding Fourier Transform of the Ge/Cu_3Ge interface of a suspended Ge NW heated using H_a heating process showing an orientation relationship potentially compatible with Ge (111)//Cu_3Ge (211), as observed by.[S1] In addition, Fig.(S2.a) shows that the interface isn't flat as it appeared in Fig.(1,2) and the Cu_3Ge
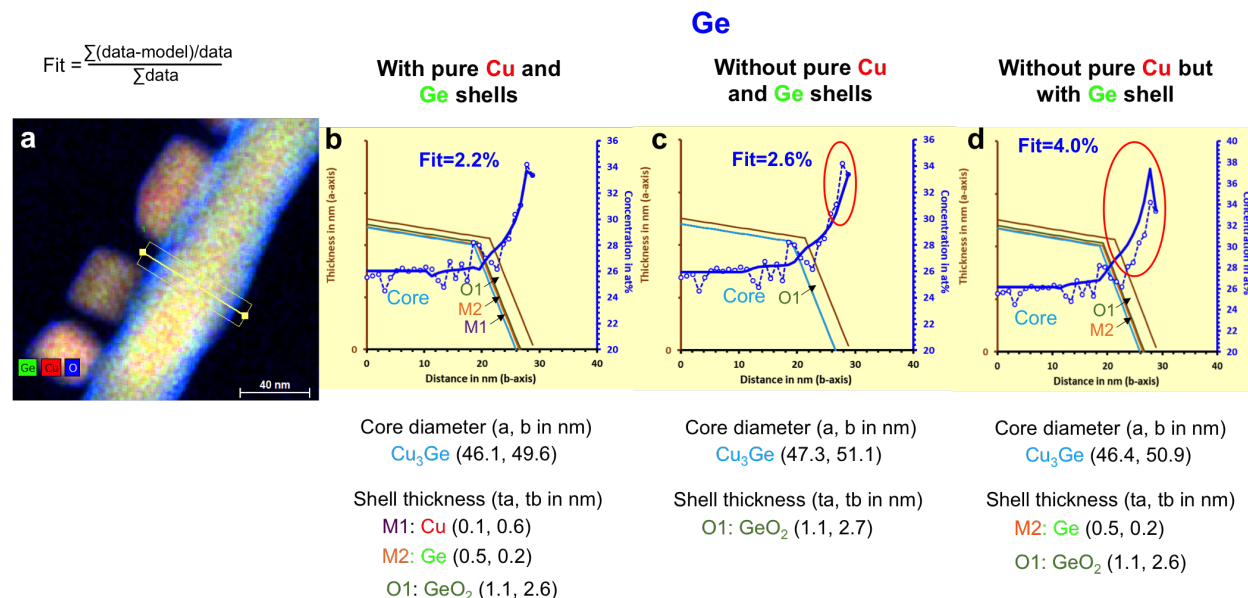
starts to form first at the NW surface.

Figure S3: *a* EDX hypermap of the Cu₃Ge segment showing the reconstructed region. *b*, *c* and *d* shows a comparison of model and quantified experimental data with and without pure Cu and Ge layers.
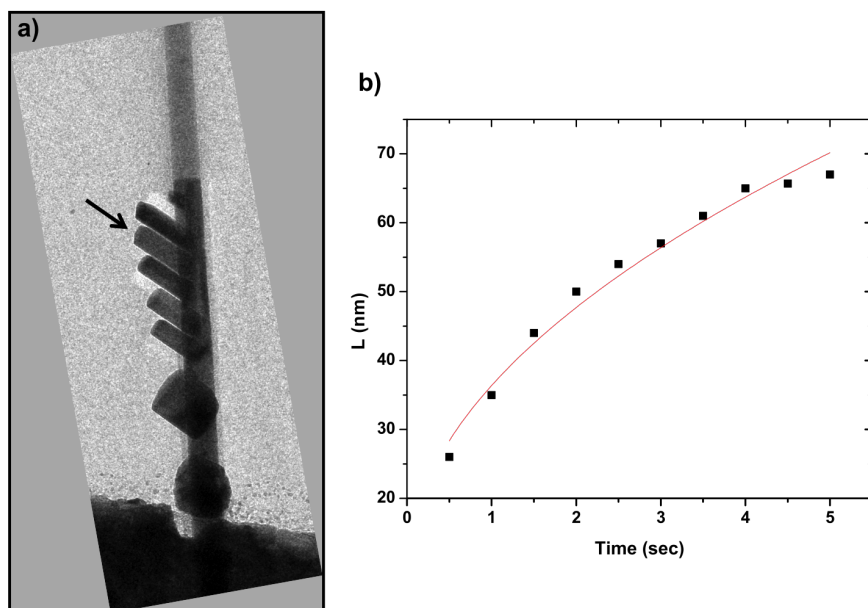

Figure S4: a) TEM image showing the sample heated using in-situ H$_b$ at 410°C. b) The length of the germanide crystal (indicated with an arrow) versus time at 410°C.
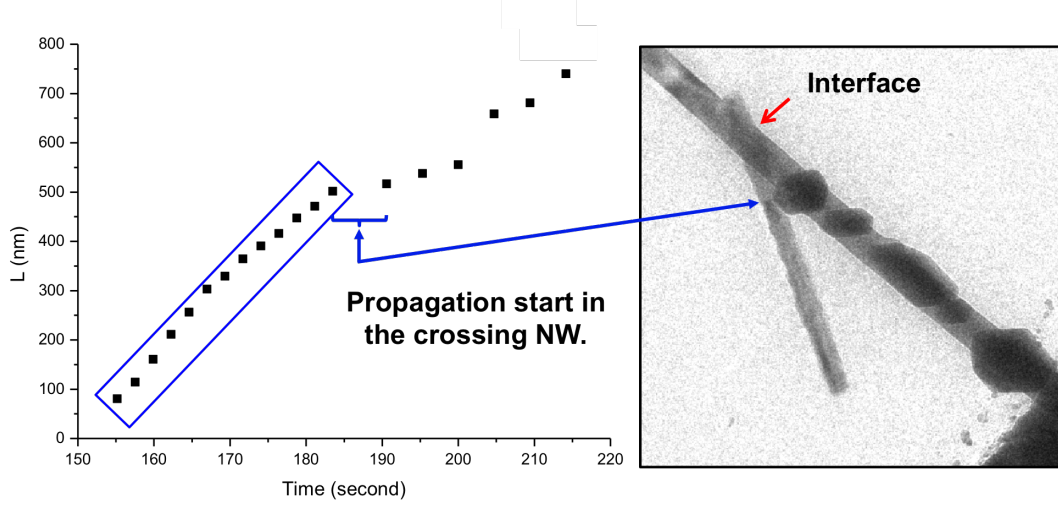
Figure S5: Illustration of the change in the germanide propagation speed when the propagation enters in the crossing NW .

In order to determine the atomic structure of the protruding crystals that appeared at 600°C in H_b experiment, selected area precession electron diffraction tomography was performed on the longest protruded crystal (see selected region in Fig.(3.c)). The precession angle of the electron beam was 1.25°, in order to limit dynamical effects. 41 precession electron diffraction (PED) patterns were recorded, from sample holder tilt angle $\alpha = -20°$ to $+ 20°$, with a step of 1°. The intensities of the different reflections were extracted and analyzed using PETs and JANA software.[S2] Slices of the reciprocal space are presented in.[S3] A hexagonal unit cell was determined, with parameters a = b = 2.6 Å, c = 4.2 Å. Reflection conditions were compatible with space group $P6_3/mmc$ (hkl : l = 2n). A structural model was determined from 14 independent reflexions using "ab initio" direct method calculations. The completeness was 88% for a resolution of 0.8 Å. It led to the disordered hexagonal compact Cu_5Ge structure already mentioned in the literature.[S4]
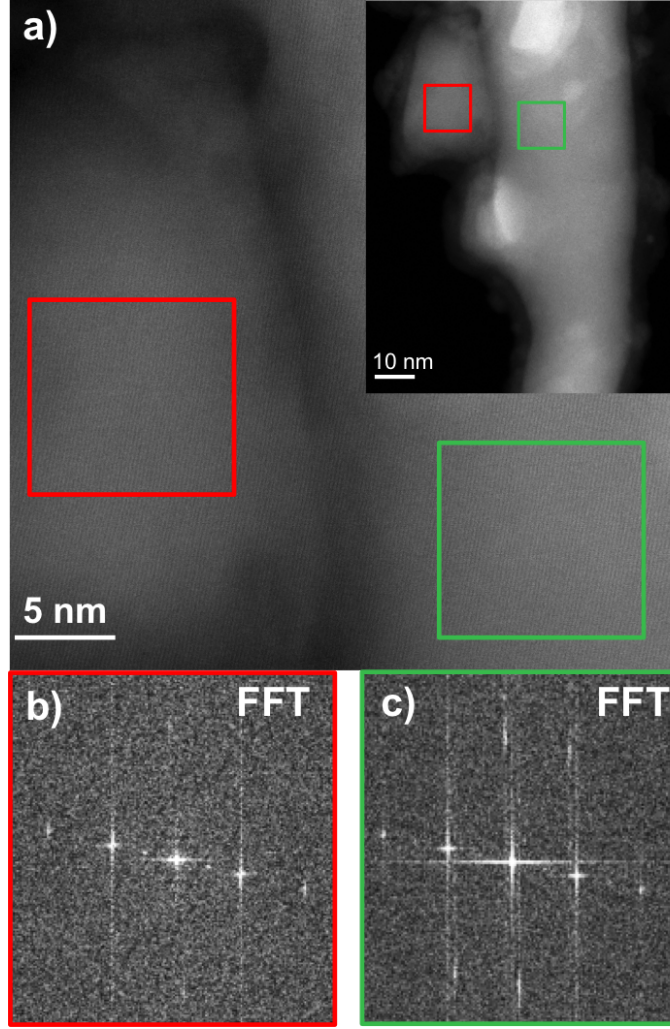
Figure S6: a) High resolution HAADF-STEM image of a transformed NW after H_a heating process. The inset HAADF-STEM image in a shows a zoom out of the represented parts in a. b) and c) Corresponding Fourier Transform of the selected parts in a, respectively, showing an epitaxial growth of the Cu_3Ge protruding crystal with respect to the Cu_3Ge NW core.

III. Copper intrusion in Ge NW

In this section, we present a basic calculation allowing to estimate the dominant diffusing species between Cu and Ge atoms, based on the experimental data of Fig.(2.a,d). After the germanide phase formation, we noticed that the NW diameter increases only with few nm. Therefore, to simplify the calculation we assume that the diameter didn't change after Cu_3Ge phase formation.
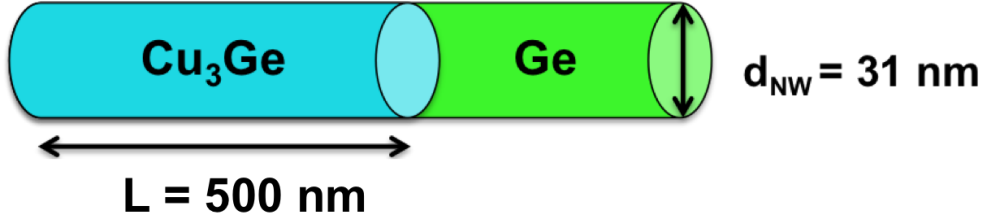
Number of Ge atoms/nm^3:

Figure S7: Schematic illustrating the section of the transformed Ge NW before and after H$_a$ and H$_b$ heating experiments.

$$C_{Ge} = \frac{Z}{V_{Ge}} = \frac{8}{(0.565)^3} = 44.35 \ atom/nm^3$$

Volume of the NW segment exchanged into Cu$_3$Ge:

$$V = \pi R^2 L = \pi \times (15.5)^2 \times 500 = 3.78 \ 10^5 \ nm^3$$

Number of Ge atoms present in the NW segment before it exchanges to Cu$_3$Ge is :

$$N_{Ge}^i = 44.35 \times 3.78 \ 10^5 = 1.67 \ 10^7 \ atom$$

In the orthorhombic Cu$_3$Ge phase structure, the lattice points per unit cell are : Cu (Z = 6) and Ge (Z = 2) and the structure volume V = 0.457 $\times$ 0.527 $\times$ 0.42 = 0.101 nm^3. Therefore, the number of Ge and Cu atoms in the Cu$_3$Ge phase/volume are :

$$C'_{Ge} = \frac{Z_{Ge}}{V} = \frac{2}{0.101} = 19.8 \ atom/nm^3 \ ; \quad C_{Cu} = \frac{Z_{Cu}}{V} = \frac{6}{0.101} = 59.4 \ atom/nm^3$$

The number of Ge and Cu atoms present in the Cu$_3$Ge segment (shown above) are :

$$N_{Ge}^f = 19.8 \times \ 3.78 \ 10^5 = 7.48 \ 10^6 \ atom \ ; \quad N_{Cu} = 59.4 \times \ 3.78 \ 10^5 = 2.24 \ 10^7 \ atom$$

So, from the N_{Ge}^i and N_{Ge}^f values we could estimate the number of Ge atoms that diffused from the NW to the Cu pad grain boundaries.

$$N_{Ge}^{diff} = N_{Ge}^i - N_{Ge}^f = 1.67 \ 10^7 - 7.48 \ 10^6 = 9.22 \ 10^6 \ atom \sim 10^7 \ atom \tag{S1}$$

To estimate the order of magnitude of Cu atoms introduced into the Ge segment comparing to the Ge atoms diffuse into the Cu grain boundaries during the Cu_3Ge phase formation we write:

$$\frac{N_{Cu}}{N_{Ge}^{diff}} = \frac{2.24 \ 10^7}{10^7} = 2.24 \tag{S2}$$

Therefore, we could conclude that the dominant diffusing species is Cu atoms during the Cu_3Ge phase formation.

IV. Diffusion Model

Different models[S5–S8] were established in a way to fit the resulting data found in metal-Si NW solid-state reactions. However, all the presented models rely on the same potential limiting steps that have been experimentally demonstrated to limit the silicide growth rate. One can observe that the models[S5,S6,S8] are established based on Deal and Grove model,[S9] certainly in different manners but keeping the same assumptions on which the model relies. Instead of presenting Tang et al[S8] model, which is an extension of the Deal and Grove model[S9] to Si NWs, we prefer to directly translate the Deal and Grove to what we have studied. So in the following an extension of the Deal and Grove model to the diffusion of germanium atoms into the metal contact is presented.

Due to geometrical constraints, the deposited metal does not surround the NW but covers the NW over a surface S_3 which includes half of the NW radius that is to say, $S_3 \sim \pi R 2 L_b$, where $2L_b$ is the length of the deposited contact along the axial direction of the NW and R is the radius of the NW, see Fig.(S8). Then the structure is heated in-situ in a TEM

microscope in order to form a germanide phase, noted G in Fig.(S8). During heating, both Cu and Ge atoms diffuse in the NW creating a germanide phase that extends on both sides of the NW and L is the length of the formed germanide phase.

Three steps can be distinguished in the reaction :

1. The simultaneous incorporation of Ge atoms in the germanide phase and diffusion channel at the Ge NW/germanide interface, respectively.

2. The diffusion from the Ge NW/germanide interface to the germanide/metal reservoir.

3. The diffusion of Ge atoms into the metal reservoir at the germanide/metal reservoir.

This model does not account for self-diffusion within the metal contacts and the Ge nanowire. Let us examine each step in turn.

1. Incorporation of Ge atoms in the germanide phase and into the diffusion channel at the Ge NW/germanide interface:

   It should be realized that all models in literature suppose that it is the diffusion of metal atoms that limit the reaction rate. One reason for this choice is that what we see during the reaction, i.e. the advancement of the reaction interface, has to be related to the arrival of metal atoms. It is this certainty that allows to construct a relation between the formed length of the germanide segment and the amount of atoms that arrived to form it. On the other hand, we cannot visualize the semiconductor atoms going back into the reservoir during the reaction (they are diluted in the metal reservoir as we showed in Fig.4). It is therefore not so obvious to write equations describing Ge as the rate limiting step, since the Ge atoms that form the germanide part do not have to diffuse to that location, they are already present.

   In section IV, we evaluated the number of Ge atoms per volume in the initial NW, being 44.35 atoms.nm^{-3} and in the created germanide segment being 19.8 atoms.nm^{-3}. Since the volume of the NW often expands a bit, we can estimate that roughly half of the Ge

atoms of the initial NW need to diffuse out, and half create the germanide phase. This assumption allows us to state that the number of incorporated Ge atoms is equal to the number of Ge atoms diffusing into the reservoir. In other words, the incorporation of Ge atoms into the germanide phase equals the amount of atoms incorporated into the diffusion channel.

As done for the Deal and Grove model in the steady state regime, the flux of incorporated atoms is given by :

$$J_1 = k_1(C_{res} - C_0) \tag{S3}$$

where k_1 is the incorporation rate constant of Ge atoms in the germanide phase. C_{res} and C_0 represent the local concentration of Ge atoms in the Ge reservoir (the NW) - this is normally a known value, as was C^* in the Deal and Grove model - and at the Ge NW/germanide interface, respectively.

During the time dt, the number dN_1 of incorporated Ge atoms in the germanide phase, is equal to :

$$dN_1 = I_1 dt = J_1 S_1 dt = k_1(C_{res} - C_0)\pi R^2 dt \tag{S4}$$

where I_1 is the Ge incorporation rate.

These Ge atoms create a thickness dL of germanide. If N is the number of Ge atoms contained in a unit cell of germanide, the volume $S_1 dL$ contains $NS_1 dL = dN_1$ atoms. So we have the equation :

$$NdL\pi R^2 = I_1 dt \tag{S5}$$

2. Diffusion through the germanide segment : The next step governing the germanide propagation, is the diffusion of dissolved atoms through the germanide segment to the germanide/Cu interface. As, we consider two diffusion paths, the total transport rate of Ge atoms I_2, will include two terms, one due to volume diffusion I_2^v and one due to

surface diffusion I_2^s.

$$I_2^v = J_2^v . S_2^v = D^v \frac{C_0 - C_1}{L} . S_2^v \quad \text{with} \quad S_2^v = \pi R^2 \tag{S6}$$

$$I_2^s = J_2^s . S_2^s = D^s \frac{C_0 - C_1}{L} . S_2^s \quad \text{with} \quad S_2^s = 2\pi \delta R \tag{S7}$$

So during the time dt, the number dN_2 of Ge atoms diffusing in or on the germanide segment is given by :

$$dN_2 = \pi R (2\, D^s \delta + D^v R) \frac{C_0 - C_1}{L} dt \tag{S8}$$

D^s is the diffusion coefficient (cm^2/s) of Ge atoms through the surface segment to the germanide/Cu interface. C_1 is the local concentration of Ge atoms at the germanide/Cu interface, L is the segment length and δ is the thickness of the surface diffusion layer where both Ge and Cu atoms diffuse through.

3. The diffusion of the Ge atoms into the Cu reservoir at the germanide/Cu interface. With notations similar to the first step, during the time dt, dN_3 the number of Ge atoms diffusing at the germanide/Cu interface is equal to :

$$dN_3 = I_3 dt = J_3 S_3 dt = D_3 \frac{C_1 - C'}{L_b} 2\pi R L_b dt \tag{S9}$$

Here we choose the diffusion length of Ge in the Cu reservoir to be approximately equal to L_b to simplify the equations. Indeed, we observed in Fig.4 that Ge diffused sideways into the Cu reservoir along distances on the order of L_b.

In steady state conditions and without accumulation of Ge atoms in the system, all the atom currents i.e. intensities are equal ($I = I_1 = I_2 = I_3$), and similarly as in the Deal Grove model, the intensity I can be expressed as a function of C_{res} to obtain an

equation depending on L:

$$I = \frac{\pi R C_{res}}{\frac{1}{Rk_1} + \frac{L}{2D^s\delta + D^v R} + \frac{1}{2D_3}}$$ (S10)

$$\frac{dL}{dt} = \frac{I}{N\pi R^2}$$ (S11)

Replacing I in this last equation, one obtains a differential equation in L similar to the one obtained in the Deal and Grove model. The big difference with the original Deal and Grove model is that now the variables A and B are a function of the NW radius R.

$$\frac{dL}{dt} = \frac{\frac{C_{res}}{N}}{\frac{1}{k_1} + \frac{L}{2D^s\frac{\delta}{R}+D^v} + \frac{R}{2D_3}} = \frac{B}{A + 2L}$$ (S12)

Where $B = 2(2D^s\frac{\delta}{R} + D^v)\frac{C_{res}}{N}$ and $A = 2(2D^s\frac{\delta}{R} + D^v)(\frac{1}{k_1} + \frac{R}{2D_3})$

The Eq.(S12) was analytically solved to relate the propagation length L to the propagation time t :

$$L = \frac{A}{2}(\sqrt{1 + \frac{(t+\tau)}{\frac{A^2}{4B}}} - 1) \quad \text{with} \quad \tau = \frac{L_0{}^2 + AL_0}{B}$$ (S13)

τ takes in account any germanide thickness at the start of the propagation; L_0 is the germanide length at t = 0. So if L_0 is taken as the origin of the x-axis, one has :

$$L = (\sqrt{\frac{A^2}{4} + Bt} - \frac{A}{2})$$ (S14)

Two limiting cases can be distinguished.

$$\text{When} \quad t >> \frac{A^2}{4B} \quad x \sim \sqrt{B.t} \quad \text{This is the parabolic regime.} \quad \text{(S15)}$$

$$\text{When} \quad t << \frac{A^2}{4B} \quad \Longrightarrow \quad x \sim \frac{B}{A}t \quad \text{This is the linear regime.} \quad \text{(S16)}$$

The rate constants B and B/A similar to Deal-Grove parameters are determined by fitting

the experimental growth data. C_{res} and N are known, B and B/A allow to determine the physical constants D^s, D^v and a mixture of k_1 and D_3.

The weakness of the model is the impossibility to predict initial stage of the germanide growth as it is assuming a steady state regime.

In fact the different regimes can be more easily understood by looking at equation (S12).

If the incorporation of Ge atoms at the Ge NW/germanide interface is the limiting factor, k_1 will be very small and it will be the main factor in eq.(S12) . L will vary linearly with time and not depend on NW radius.

If the reaction at the germanide/Cu interface is the limiting factor, the reaction at this interface will be very slow and the diffusion constant D_3 will be very small compared to the other physical constants and it will be the main factor in eq.(S12) and L will vary linearly with time and L will vary as R^{-1}.

If the diffusion along the germanide section is the limiting factor, the dominant factor in eq.(S12) will be the term dependent on L. So when solving eq.(S12), L will vary as a square root as a function of time. If its volume diffusion, L will be independent of the NW radius R, if it is a surface diffusion L will vary as a function of R^{-1}. These different regimes are summarized in Table.(3).
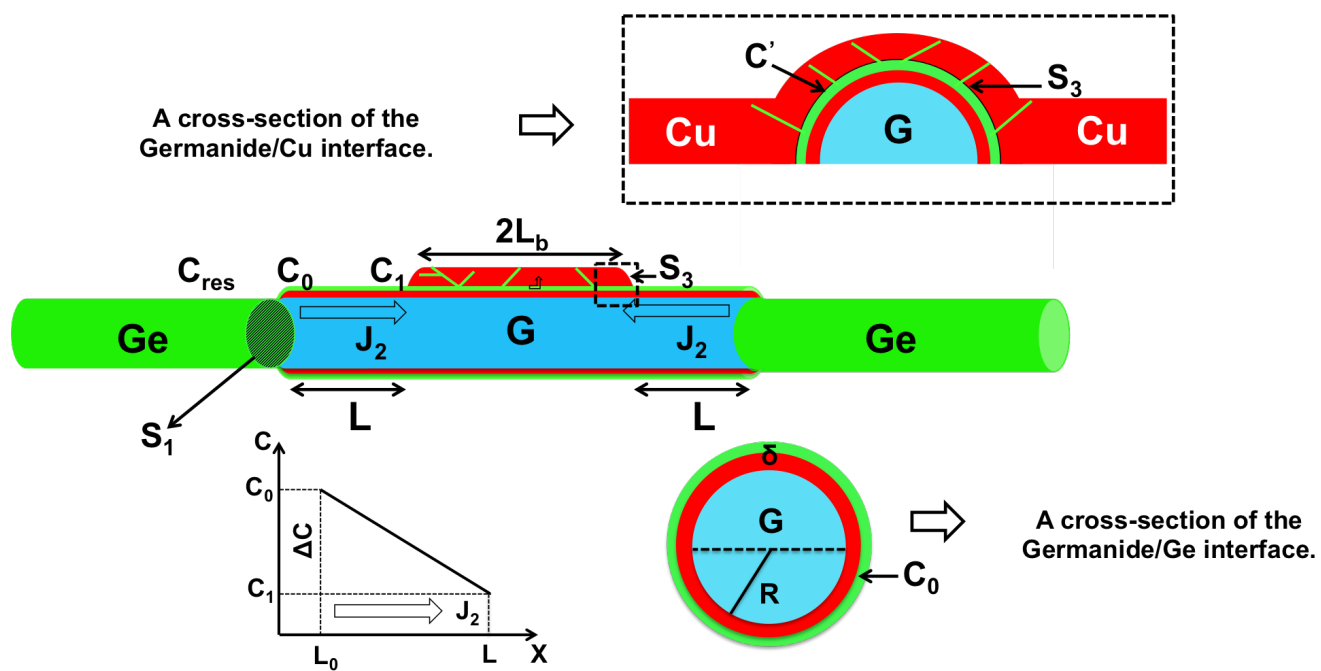
Figure S8: Schematic illustrating the different mechanisms taking place during the germanide growth.

References

(S1) Burchhart, T.; Lugstein, A.; Hyun, Y. J.; Hochleitner, G.; Bertagnolli, E. *Nano Letters* **2009**, *9*, 3739–3742.

(S2) Palatinus, L. *Institute of Physics, Prague, Czech* **2011**,

(S3) El Hajraoui, K. In-situ transmission electron microscopy studies of metal-Ge nanowire solid-state reactions. Theses, Université Grenoble Alpes, 2017.

(S4) Krusin-Elbaum, L.; Aboelfotoh, M. O. *Applied Physics Letters* **1991**, *58*, (1341–1343).

(S5) Yaish, Y. E.; Katsman, A.; Cohen, G. M.; Beregovsky, M. *Journal of Applied Physics* **2011**, *109*, 094303.

(S6) Ogata, K.; Sutter, E.; Zhu, X.; Hofmann, S. *Nanotechnology* **2011**, *22*, 365305.

(S7) Chen, Y.; Lin, Y.-C.; Huang, C.-W.; Wang, C.-W.; Chen, L.-J.; Wu, W.-W.; Huang, Y. *Nano Letters* **2012**, *12*, 3115–3120.

(S8) Tang, W.; Nguyen, B.-M.; Chen, R.; Dayeh, S. A. *Semiconductor Science and Technology* **2014**, *29*, 054004.

(S9) Deal, B. E.; Grove, A. S. *Journal of Applied Physics* **1965**, *36*, 3770–3778.